Absolute Rate Coefficient Determination and Reaction Mechanism Investigation for the Reaction of Cl Atoms with CH_2I_2 and the Oxidation Mechanism of CH_2I Radicals

Vassileios G. Stefanopoulos, Vassileios C. Papadimitriou,[†,‡] Yannis G. Lazarou,*[,§] and Panos Papagiannakopoulos*

Laboratory of Photochemistry and Kinetics, Department of Chemistry, University of Crete, Heraklion 710 03, Crete, Greece

Received: October 3, 2007; In Final Form: November 28, 2007

The gas-phase reaction of atomic chlorine with diiodomethane was studied over the temperature range 273−363 K with the very low-pressure reactor (VLPR) technique. The reaction takes place in a Knudsen reactor at pressures below 3 mTorr, where the steady-state concentration of both reactants and stable products is continuously measured by electron-impact mass spectrometry. The absolute rate coefficient as a function of temperature was given by $k = (4.70 \pm 0.65) \times 10^{-11} \exp[-(241 \pm 33)/T]$ $cm^3 molecule^{-1} s^{-1}$, in the low-pressure regime. The quoted uncertainties are given at a 95% level of confidence (2σ) and include systematic errors. The reaction occurs via two pathways: the abstraction of a hydrogen atom leading to HCl and the abstraction of an iodine atom leading to ICl. The HCl yield was measured to be ca. 55 ± 10%. The results suggest that the reaction proceeds via the intermediate CH_2I_2−Cl adduct formation, with a I−Cl bond strength of 51.9 ± 15 kJ mol^{-1}, calculated at the B3P86/aug-cc-pVTZ-PP level of theory. Furthermore, the oxidation reactions of CHI_2 and CH_2I radicals were studied by introducing an excess of molecular oxygen in the Knudsen reactor. HCHO and HCOOH were the primary oxidation products indicating that the reactions with O_2 proceed via the intermediate peroxy radical formation and the subsequent elimination of either IO radical or I atom. HCHO and HCOOH were also detected by FT-IR, as the reaction products of photolytically generated CH_2I radicals with O_2 in a static cell, which supports the proposed oxidation mechanism. Since the photolysis of CH_2I_2 is about 3 orders of magnitude faster than its reactive loss by Cl atoms, the title reaction does not constitute an important tropospheric sink for CH_2I_2.

1. Introduction

Several iodinated compounds have been detected in considerable concentrations over coastal areas and are lately considered as main contributors to tropospheric ozone loss and in a minor extent to stratospheric ozone depletion.[1,2] Recent studies have also shown that these compounds emitted by marine algae are partially converted by sunlight into aerosol particles, and this process could have significant effects on climate.[3,4] Iodinated compounds are removed from the troposphere via photolysis as well as via their reactions with OH radicals and Cl atoms. Although OH radical reactions are predominant in the troposphere, Cl atom reactions with iodinated compounds are expected to be also important, because of the substantial Cl concentrations over the marine boundary layer,[5−7] where iodinated compounds are emitted, and the higher reactivity of Cl atoms compared to OH radicals with the majority of organic compounds.[8]

Among the iodinated organic compounds detected in the troposphere, diiodomethane (CH_2I_2) is considered to be an important precursor of iodine atoms because of its high photolability,[9,10] surpassed only by molecular iodine, I_2, which is considered to be 10^3 times more effective in the coastal marine boundary layer.[11,12] Recent emission measurements over coastal biota around Mace Head have shown that CH_2I_2 is among the primary iodinated species released, with an emission rate as high as 1 ng s^{-1} m^{-2}.[13] However, gas-phase kinetic data for CH_2I_2 reactions with the primary atmospheric reactants OH radicals and Cl atoms are very limited; no data are available for OH radicals and only preliminary results were reported for Cl atoms.[14,15] In particular, the rate coefficients for the reactions

$$Cl + CH_2I_2 \rightarrow \begin{cases} HCl + CHI_2 \\ ICl + CH_2I \end{cases} \quad (1)$$

are expected to be relatively high and pressure-dependent because of the intermediate formation of a ICH_2I−Cl adduct, which was recently detected by its visible absorption in the range 405−632 nm,[16] as well as by laser induced fluorescence in the range 345−375 nm.[15] In general, experimental and theoretical studies have suggested the presence of attractive forces between Cl atoms with iodinated molecules, which may lead to adducts possessing weak I−Cl bonds.[16−24] For Cl atom reactions, pathways proceeding via adduct formation (besides direct abstraction pathways) may enhance the overall rate coefficient and affect the reaction mechanism as well as the branching ratios.

Furthermore, CH_2I radical is a key species in the atmospheric chemistry of iodinated compounds, since it is generated by

* To whom correspondence should be addressed. E-mail: lazarou@chem.demokritos.gr; E-mail: panosp@chemistry.uoc.gr.

† Earth System Research Laboratory, Chemical Science Division, National Oceanic and Atmospheric Administration, 325 Broadway, Boulder Colorado, 80305-3328.

‡ Cooperative Institute for Research in Environmental Sciences, University of Colorado, Boulder Colorado, 80309.

§ Institute of Physical Chemistry, National Centre for Scientific Research "Demokritos", Aghia Paraskevi GR-153 10, Attiki, Greece.

10.1021/jp7096789 CCC: $40.75
Published on Web 01/26/2008

photolysis and chemical reactions involving the most abundant CH_3I and CH_2I_2

$$CH_2I_2 \xrightarrow{h\nu} CH_2I + I$$

$$X + CH_2I_2 \rightarrow CH_2I + IX$$

$$X + CH_3I \rightarrow CH_2I + HX$$

where $X = OH$ or Cl.

The oxidation of CH_2I radicals in the troposphere is expected to occur via the initial association with O_2 leading to ICH_2OO radicals, which subsequently follow a degradation mechanism in analogy to other halogenated peroxy radicals.[25,26] It has been reported that the oxidation reaction occurs exclusively via the reaction

$$CH_2I + O_2 \rightarrow IO + HCHO \qquad (2)$$

by observing the appearance of IO product using cavity ring-down spectroscopy (CRDS).[27] However, in another study of the above reaction by using photoionization mass spectrometry, it was shown that, beside IO radicals, I atoms are also generated, and furthermore, they constitute the main reaction products.[28] The IO yields for the reactions of longer iodoalkyl radicals (generated by H atom abstraction by Cl atoms from the corresponding iodoalkanes) with O_2 were also recently measured by CRDS technique to be rather low (0.05−0.15).[29] The rate coefficient for reaction 2 has been measured to be $k_{298} = (4.0 \pm 0.4) \times 10^{-13}$ cm^3 molecule^{-1} s^{-1} (independent of pressure and temperature in the ranges 5−80 Torr and 278 − 313 K)[27] and $k_{298} = (1.6 \pm 0.2) \times 10^{-13}$ cm^3 molecule^{-1} s^{-1} (independent of pressure in the range 0.6−6 Torr).[30] In a more recent study, the temperature dependence of $k_2 = (1.39 \pm 0.01) \times 10^{-12}$ (T/300 K)$^{-1.55 \pm 0.06}$ cm^3 molecule^{-1} s^{-1} was determined in the range 220−450 K.[28]

The aim of the present study was the kinetic and mechanistic investigation of the gas-phase reaction of Cl atoms with CH_2I_2 over the temperature range 273−363 K at low-pressure conditions. The absolute rate coefficients and the primary reaction pathways were determined by using a molecular flow system consisting of a very low-pressure Knudsen reactor (VLPR) coupled to a quadrupole mass spectrometer.[31] Furthermore, the oxidation reaction pathways of the primary iodinated radicals CH_2I and CHI_2 were investigated by introducing molecular O_2 in the Knudsen reactor through a third inlet. In addition, the oxidation pathways of the CH_2I radical were investigated by the sunlight photolysis of gaseous CH_2I_2 in the presence of excess O_2, followed by FT-IR product analysis. Finally, DFT calculations were performed to determine the C−H and C−I bond strengths and the thermochemistry of all reaction pathways, including the adduct formation and the radical oxidation processes.

2. Experimental Section

The reaction of chlorine atoms with diiodomethane in the gas phase was studied by using a continuous flow−molecular beam system equipped with a quadrupole mass spectrometer, which has been described in detail previously.[31] The double-wall Knudsen reactor ($V = 45$ cm^3) was coated with a thin film of Teflon (FEP 121A, DuPont) to suppress wall reactions, and its temperature was controlled by liquid circulation through the outer jacket (±0.1 K). The escape rate coefficients for various species were determined by monitoring the first-order decay of their mass spectrometric signal after a fast halt of the flow. The escape aperture diameter was 5 mm and the measured escape rate coefficients were given by the expression $k_{esc,S} = 4.97(T/M)^{1/2}$ s^{-1}, where T is the reactor temperature and M is the molecular weight of species S. The oxidation experiments were performed in a larger Knudsen reactor ($V = 168$ cm^3) equipped with a third inlet for the admission of O_2 and using a smaller escape aperture of 2 mm, in order to increase the residence time of the primary reaction products. Thus, the yields of secondary oxidation reactions were sufficiently enhanced in order to allow the mass spectrometric detection of oxidation products. During the title reaction rate coefficient measurements, the total pressure inside the reactor was always below 3 mTorr with an average value throughout the experiments of about 1 mTorr, while for the radical oxidation experiments by O_2, the total pressure reached a maximum of 15 mTorr.

TABLE 1: Electron Impact Mass Spectra of CH_2I_2, ICl, CH_2ClI, HCOOH, and HCHO Taken at an Electron Energy of 19 eV[a]

CH_2I_2					
m/e	127	141	254	268	
fragment	I^+	CH_2I^+	I_2^+	$CH_2I_2^+$	
relative intensity	32	100	2	30	
ICl					
m/e	127	162	164		
fragment	I^+	$I^{35}Cl^+$	$I^{37}Cl^+$		
relative intensity	100	51	14		
CH_2ClI					
m/e	49	51	127	176	178
fragment	$CH_2{}^{35}Cl^+$	$CH_2{}^{37}Cl^+$	I^+	$CH_2{}^{35}ClI^+$	$CH_2{}^{37}ClI$
relative intensity	100	30	25	13	4
HCOOH					
m/e	28	29	45	46	
fragment	CO^+	HCO^+	$HCOO^+$	$HCOOH^+$	
relative intensity	12	45	45	100	
HCHO					
m/e	28	29	30		
fragment	CO^+	HCO^+	$HCHO^+$		
relative intensity	5	59	100		

[a] Intensities are reported relative to the intensity of the most prominent mass peak.

Chlorine atoms were generated by flowing a mixture of 30% Cl_2/He through a quartz tube, which is enclosed in a 2.45 GHz microwave cavity operating at 35 W. The Cl_2 dissociation yield was not complete (ca. 50%) and was continuously determined by monitoring its parent peak at *m*/*e* 70. The steady-state concentration of chlorine atoms was measured by monitoring the mass peak at *m*/*e* 35. The electron ionization energy was kept low at 19 eV to suppress the fragmentation of HCl to Cl^+ (*m*/*e* 35) to negligible levels (ca. 0.03%). The mass spectrometric fragmentation of Cl_2 was also taken into account and its contribution was always subtracted from the intensity of the peak at *m*/*e* 35.

The fragmentation mass spectra of all relative species are shown in Table 1. The fragmentation pattern of CH_2I_2 at 19 eV showed four major peaks at *m*/*e* 127 (I^+), 141 (CH_2I^+), 252 (I_2^+) and 268 ($CH_2I_2^+$); the highest peak at *m*/*e* 141 was selected to monitor the concentration of CH_2I_2 reactant (free of any contribution from stable reaction products).

The reactants steady-state concentrations inside the reactor were determined by monitoring the signal intensity I_M of the selected fragment ion peak, which is given by the expression $I_M = a_M F_M = a_M k_{esc,M} V [M]$, where a_M corresponds to the mass spectrometric calibration factor of each species, F_M to the flow rate (molecule s^{-1}), V to the reactor volume (cm^3), and $k_{esc,M}$ to the escape rate coefficient (s^{-1}). The calibration factor a_M of both reactants was accurately determined by plotting I_M versus F_M. The flow rate (F_M) of stable reactants from known buffer volumes through selected capillaries was obtained by monitoring the pressure drop in the buffer volume as a function of time. The Cl_2/He mixture and CH_2I_2 molecules were flowing through 1 mm × 146 cm and 1.5 mm × 28 cm capillaries, respectively. In particular, the flow rate of chlorine atoms (F_{Cl}) was derived by assuming a mass balance for all chlorinated species in the discharge tube and the reactor, in the absence of any reactants. The mass balance is given by the expression: $2\Delta F_{Cl_2} = F_{Cl} + F_{HCl}$, where ΔF_{Cl_2} is the change in the flow rate of Cl_2 when the microwave discharge was turned on, while F_{Cl} and F_{HCl} are the flow rates of Cl and HCl, respectively. The mass spectrometric sensitivity of Cl atoms was determined relative to that for HCl, whose a_{HCl} factor was determined by calibration plots of a mixture of 5% HCl in He. The ratio (a_{HCl}/a_{Cl}) was determined by titration experiments using the simple reaction of Cl atoms with hexane, n-C_6H_{14}, and it was found to be 1.3 ± 0.1. Thus, the flow rate F_{Cl} was obtained by using the expression: $F_{Cl} = (2\Delta F_{Cl_2}/[1 + I_{HCl}/(a_{HCl}/a_{Cl} \times I_{Cl})])$, and a typical plot of the intensity I_{Cl} as a function of F_{Cl} is shown in Figure S1 in Supporting Information.

The ranges of the steady-state concentrations of Cl and CH_2I_2 reactants were $9 \times 10^{10}-2.8 \times 10^{12}$ molecule cm^{-3}, and $1 \times 10^{11}-2.5 \times 10^{13}$ molecule cm^{-3}, respectively. The mass spectral intensities were measured with an uncertainty of ca. 5%, thus the ratio $[M]_o/[M] = I_{M,o}/I_M$ was determined with an accuracy of ca. 7%.

The photolysis runs were carried out in a cylindrical cell with a length of 8 cm and a diameter of 4 cm with NaCl windows attached to both ends. The cell was filled with 1 Torr of CH_2I_2 and ca. 400 Torr of O_2. It was then exposed either to direct sunlight or to the light emitted by a Mercury UV lamp (Philips HPL-N, 125 W, $\lambda_{max} = 366$ nm). IR spectra of the cell contents were taken before the photolysis as well as during the photolysis at intervals of 15, 30, and 60 min, with a resolution of 1 cm^{-1} in the range 600−4000 cm^{-1}, by a Perkin-Elmer SPECTRUM BX FT-IR spectrometer. The IR spectrum of HCHO was taken after a brief heating of solid paraformaldehyde $(H_2CO)_3$ which was previously deposited inside the cell and degassed.

The chemicals used were commercially available and their stated purities were: CH_2I_2 (99%, Aldrich), Cl_2 (99.5%, Linde), HCl (99.8, Linde), He (99.9993%, Linde), O_2 (99.995%, Linde), HCOOH (98%, Merck) and paraformaldehyde $(H_2CO)_3$ (95%, Fluka). CH_2I_2 and Cl_2 were degassed several times at 77 K prior to use.

3. Results

Rate Coefficient Measurements. The reaction of Cl atoms with CH_2I_2 may proceed via the following reaction pathways

$$Cl + CH_2I_2 \rightarrow HCl + CHI_2 \quad (1a)$$

$$Cl + CH_2I_2 \rightarrow ICl + CH_2I \quad (1b)$$

$$Cl + CH_2I_2 \rightarrow I + CH_2ClI \quad (1c)$$

while the most probable secondary reactions are

$$Cl + ICl \rightarrow Cl_2 + I \quad (3)$$

$$CHI_2 + Cl_2 \rightarrow CHClI_2 + Cl \quad (4)$$

$$CH_2I + Cl_2 \rightarrow CH_2ClI + Cl \quad (5)$$

Mass spectrometric analysis of the reaction products revealed the appearance of new peaks at m/e 36 (HCl^+) and m/e 162 (ICl^+), followed by a decrease of reactant peaks at m/e 35 (Cl^+) and m/e 141 (CH_2I^+), and an increase of the peak at m/e 70 (Cl_2^+). In addition, the ratios $I_{HCl}/\Delta I_{Cl}$ and $I_{ICl}/\Delta I_{Cl}$ were found to increase linearly with CH_2I_2 concentration, which is a clear evidence that both HCl and ICl are primary reaction products. No peaks attributable to $CHClI_2$ (at m/e 175, $[CHClI]^+$) and CH_2ClI (at m/e 49, $[CH_2Cl]^+$) were detected (Table 1), indicating the absence of primary reaction 1c, as well as of secondary reactions 4 and 5. However, the formation of ICl product was found initially to increase sharply with Cl atoms concentration reaching a maximum at $[Cl] \approx 5 \times 10^{11}$ molecule cm^{-3}, followed by a gradual decrease as shown in Figure 1. This constitutes a clear evidence that secondary reaction 3 takes place, resulting in the consumption of ICl and the formation of Cl_2 and I products, whose intensity increases at $m/e = 70$ and 127, respectively. Reaction 3 has been measured to be relatively fast, with a rate coefficient $k_3 = 1.0 \times 10^{-11}$ cm^3 $molecule^{-1}$ s^{-1},[32] comparable with the magnitude of the title reaction. Thus, the rate coefficient measurements could not accurately rely on the variation of Cl atoms concentration versus the CH_2I_2 concentration, as was done in previous studies.[31] Instead, the rate coefficient was measured by monitoring the variation of CH_2I_2 concentration as a function of Cl atoms concentration, which avoids any interference from other primary or secondary reactions of Cl atoms as well as from any wall loss of Cl atoms. By this treatment, complications arising from the possible sticking of CH_2I_2 on the reactor walls are also avoided, since only the change of the gas-phase CH_2I_2 concentration by the presence of Cl atoms is employed, as shown below.

In particular, the steady-state for CH_2I_2 molecules is given by the expression

$$\Delta[CH_2I_2]k_{esc,CH2I2} = k_1[Cl][CH_2I_2] \quad (I)$$

where $\Delta[CH_2I_2] = [CH_2I_2]_o - [CH_2I_2]_r$, $k_{esc,CH2I2}$ is the escape rate of CH_2I_2 molecules, and [Cl] and $[CH_2I_2]$ are the reactants concentrations when both are present in the reactor. Rearrangement of expression I gives

$$(R - 1)k_{esc,CH2I2} = k_1[Cl]$$

where $R = [CH_2I_2]_o/[CH_2I_2]_r = I_{141,o}/I_{141,r}$ and subscripts o and r denote the absence or presence of Cl atoms, respectively. The linear least-squares fits of the data to expression I yield the rate coefficient k_1. The quoted uncertainties represent the 2σ precision of the fits (95% level of confidence). A typical plot of the above equation at $T = 303$ K is presented in Figure 2, and typical experimental data for reaction 1 are presented in Table 2.

Experiments were performed at four different temperatures (273, 303, 333, and 363 K), and the obtained absolute rate coefficients were $k_{273} = (1.94 \pm 0.12) \times 10^{-11}$ cm^3 $molecule^{-1}$ s^{-1}, $k_{303} = (2.12 \pm 0.06) \times 10^{-11}$ cm^3 $molecule^{-1}$ s^{-1}, $k_{333} = (2.31 \pm 0.08) \times 10^{-11}$ cm^3 $molecule^{-1}$ s^{-1}, and $k_{363} = (2.40 \pm 0.20) \times 10^{-11}$ cm^3 $molecule^{-1}$ s^{-1}. The Arrhenius plot of the experimental rate coefficients is presented in Figure 3. Linear least-squares analysis of the temperature dependence data yields

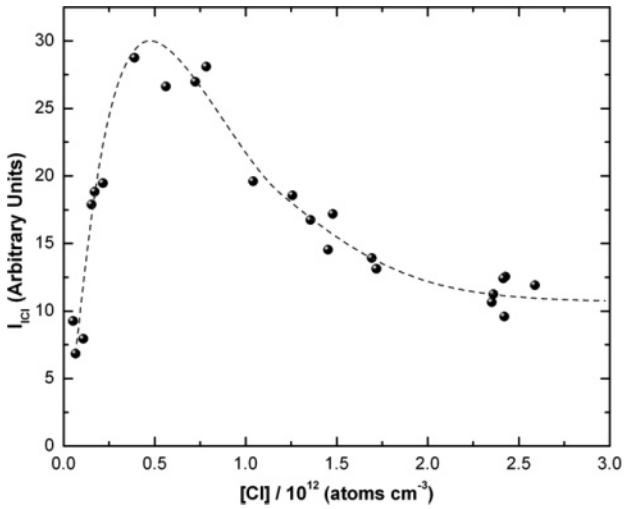

Figure 1. Plot of ICl mass spectrometric intensity versus Cl atoms concentration at 303 K. The dashed line is only for illustrating the trend and does not correspond to any fit expression of the data.

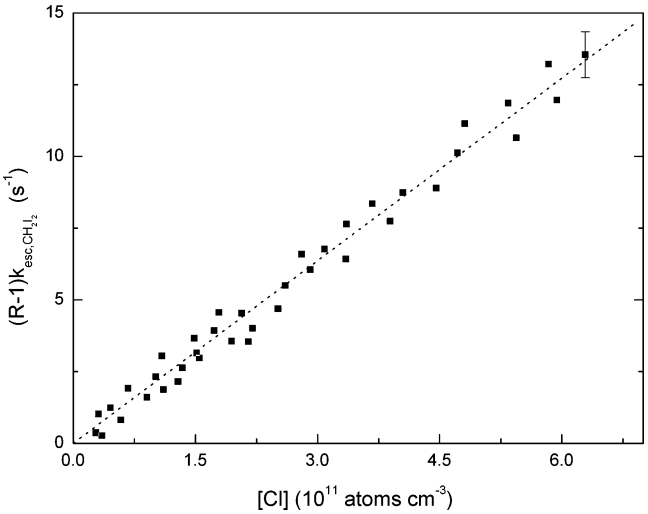

Figure 2. Plot of $(R-1)k_{esc,CH2I2}$ versus [Cl] at $T = 303$ K. The linear least-squares analysis of the data yield $k_1(T = 303\ \text{K}) = (2.12 \pm 0.20) \times 10^{-11}$ cm^3 molecule^{-1} s^{-1}. The quoted uncertainties (and the depicted error bar) include the estimated systematic errors of the rate coefficient measurements.

the activation energy E_a and the Arrhenius factor A for reaction 1. The temperature-dependent rate coefficient was determined to follow the expression

$$k_1(\text{T}) = (4.70 \pm 0.50) \times 10^{-11} \exp[-(241 \pm 33)/T]\ \text{cm}^3\ \text{molecule}^{-1}\ \text{s}^{-1}$$

Estimating the systematic errors in the rate coefficient measurements to be 9%[33] and including them into the pre-exponential factor leads to

$$k_1(\text{T}) = (4.70 \pm 0.65) \times 10^{-11} \exp[-(241 \pm 33)/T]\ \text{cm}^3\ \text{molecule}^{-1}\ \text{s}^{-1}$$

The uncertainty in the exponential term represents the 2σ precision of the linear least-squares analysis.

HCl Yield Measurements. The HCl yield was continuously measured by applying the steady state for HCl molecules and monitoring the variation of $\Delta[\text{HCl}]\ k_{esc,HCl}/[\text{Cl}]$ as a function of CH_2I_2 concentration, according to the expression

$$\Delta[\text{HCl}]k_{esc,\text{HCl}} = k_{1a}[\text{CH}_2\text{I}_2][\text{Cl}]$$

where $\Delta[\text{HCl}] = [\text{HCl}]_r - [\text{HCl}]_{bg}$ is the concentration difference between the HCl produced via reaction 1a and that present as a background signal. [Cl] and $[CH_2I_2]$ are the steady-state concentration for Cl atoms and CH_2I_2 molecules, respectively, and $k_{esc,HCl}$ is the escape rate coefficient for HCl species. The background HCl is generated inside the discharge tube, with a stable and reproducible signal throughout the experiments.

A typical plot for the determination of k_{1a} at $T = 303$ K is presented in Figure 4. Furthermore, the HCl yield (k_{1a}/k_1) was

TABLE 2: Typical Experimental Data for the Steady-State Concentrations of Cl Atoms and CH_2I_2 Molecules (10^{11} Molecule cm^{-3}), and $(R-1)k_{esc,CH2I2}$ (s^{-1}), Where $R = ([CH_2I_2]_o/[CH_2I_2])$ and Subscript o Denotes the Steady-State Concentration in the Absence of the Other Reactant

$[CH_2I_2]_o$	$[CH_2I_2]$	$(R-1)k_{esc,CH2I2}$	[Cl]
	$T = 273$ K		
97.36	67.67	2.20	0.92
75.91	26.04	9.60	4.55
95.93	25.21	14.06	7.57
62.22	10.04	26.05	13.91
99.71	10.99	40.46	20.97
	$T = 303$ K		
88.51	54.45	3.30	1.63
234.07	82.58	9.69	4.42
81.29	17.22	19.65	6.99
177.23	34.47	21.87	12.05
62.71	7.57	38.44	18.44
	$T = 333$ K		
77.38	40.66	5.00	2.19
76.43	35.54	6.37	3.02
69.51	25.72	9.43	3.89
76.11	21.62	13.95	5.97
93.89	11.28	40.55	19.16
	$T = 363$ K		
88.83	44.74	5.70	2.33
122.01	43.78	10.33	4.71
75.33	17.59	18.98	8.44
125.57	22.08	27.09	11.31
116.28	14.16	41.70	19.24

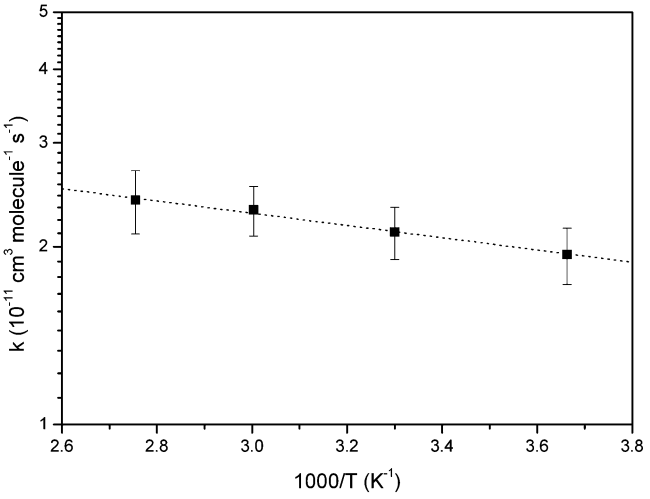

Figure 3. Arrhenius plot of k_1 (logarithmic scale) as a function of temperature (1000/T). Least-squares fit of the data (dashed line) yield $k_1(T) = (4.70 \pm 0.65) \times 10^{-11} \exp[-(241 \pm 33)K/T]$ cm^{3}molecule^{-1}s^{-1}. Error limits and quoted uncertainties include estimated systematic errors at 95% level of confidence (2σ).

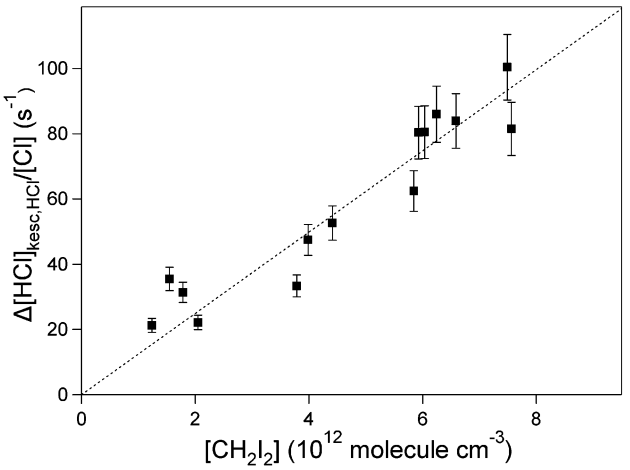

Figure 4. Plot of $\Delta[HCl]k_{esc,HCl}/[Cl]$ as a function of CH_2I_2 concentration at $T = 303$ K. The linear least-squares analysis of the data yield $k_{1a}(T = 303\ K) = (1.24 \pm 0.10) \times 10^{-11}$ cm^3 molecule^{-1} s^{-1}. The quoted uncertainty is the 2σ precision of the linear least-squares analysis. The error bars reflect the uncertainty of expression $\Delta[HCl]k_{esc,HCl}/[Cl]$ at a 95% level of confidence (2σ) and includes estimated systematic errors.

determined to be independent of temperature between 273 and 363 K, within the given uncertainty, and the average value resulted from the experimental data analysis was $k_{1a}/k_1 = 0.55 \pm 0.10$. The quoted uncertainty includes estimated systematic errors.

Iodomethyl Radical Oxidation Experiments. The reaction of CHI_2 and CH_2I radicals with O_2 molecules may proceed via the following reaction pathways:

$$CHI_2 + O_2 \longrightarrow I_2CHOO \begin{cases} \longrightarrow IO + ICHO & (6a) \\ \longrightarrow HI + ICOO \longrightarrow HI + I + CO_2 & (6b) \\ \longrightarrow OH + I_2CO & (6c) \\ \longrightarrow I + HICOO \longrightarrow I + HI + CO_2 & (6d) \end{cases}$$

$$CH_2I + O_2 \longrightarrow ICH_2OO \begin{cases} \longrightarrow IO + HCHO & (7a) \\ \longrightarrow HI + HCOO \longrightarrow HI + H + CO_2 & (7b) \\ \longrightarrow OH + ICHO & (7c) \\ \longrightarrow I + H_2COO \longrightarrow I + HCOOH & (7d) \end{cases}$$

The mechanism of the oxidation reactions of the primary CHI_2 and CH_2I radicals generated by the title reaction was investigated by introducing an excess of O_2 molecules (ca. 4×10^{14} molecule cm^{-3}) in the reaction mixture, through a third inlet of the Knudsen reactor. The addition of O_2 resulted in an increase of the mass peak at *m*/*e* 127 (I^+), and the appearance of four new mass peaks at *m*/*e* 29, 30, 44, and 46. The peak at *m*/*e* 29 (CHO^+) may be due to the fragmentation of ICHO and HCHO products of pathways 6a/7c and 7a, respectively. The peak at *m*/*e* 30 ($HCHO^+$) corresponds to HCHO product, which indicates the presence of pathway 7a, and the peak at *m*/*e* 46 ($HCOOH^+$) corresponds to HCOOH, indicating the presence of pathway 7d. In addition, the peak at *m*/*e* 44 (CO_2^+) suggests the generation of CO_2 via pathways 6b, 6d, and 7b. However, HI was not detected (at its parent peak at *m*/*e* 128) among the reaction products and this is possibly attributed to its depletion by Cl atoms with a rate coefficient of 1.11×10^{-11}.[34] In addition, no iodine monoxide IO was detected at its parent peak at *m*/*e* 143, which may be possibly due to several reasons: (a) complete fragmentation of the parent cation IO^+ leading to a contribution at *m*/*e* 127, (b) fast depletion by Cl atoms ($k_{Cl+IO} = (4.4 \pm 1.0) \times 10^{-11}$ cm^3 molecule^{-1} s^{-1}),[35] (c) its fast self-reaction with a rate coefficient $k_{IO+IO} = (9.3 \pm 1.9) \times 10^{-11}$ cm^3 molecule^{-1} s^{-1},[36] and (d) wall loss, or a combination of the above. Moreover, all reaction pathways lead to iodinated species undergoing extensive fragmentation to an intense mass peak at *m*/*e* 127 (I^+) and several overlapping peaks at low mass numbers, prohibiting a complete elucidation of the reaction mechanism by mass spectrometry alone. It should be noted that the similarity between the oxidation schemes of CHI_2 and CH_2I radicals and the prompt mass spectrometric fragmentation of iodinated species did not allow a clear identification of products from CHI_2 radical oxidation pathways. Experimental difficulties in handling pure samples of gaseous HCHO and HCOOH precluded the quantitative determination of the relative oxidation products yields.

The oxidation mechanism of CH_2I by O_2 was additionally investigated by IR spectroscopy in a static cell by using the photolysis of CH_2I_2 as the source of CH_2I radicals, in the presence of an excess of O_2. The IR spectrum before the photolysis was subtracted from all spectra to aid in the detection and identification of oxidation products. FT-IR spectra of gaseous samples of HCOOH and HCHO were also taken for comparison. Several iodine-containing products, comprising of ICH_2CH_2I (as a recombination product of CH_2I), IO, HI, and ICHO were also considered, and their IR absorption bands were taken from literature[37] or from vibrational frequencies calculated in this study. After photolysis, various new absorption bands appeared which could be attributed to the presence of HCOOH (υ_6, υ_5, υ_3, υ_2, and υ_1 bands in the ranges 1036−1250, 1700−1820, and 2800−3610 cm^{-1}, with sharp peaks at 1104 and 1775 cm^{-1}), HCHO (υ_3, υ_2, υ_1, and υ_5 bands in the ranges 1430−1820 and 2640−3080 cm^{-1}, with sharp peaks at 1501 and 1745 cm^{-1}) and CO (characteristic PR profile in the range 2055−2225 cm^{-1}). A typical FT-IR spectrum of the photolyzed mixture is shown in Figure S2 in Supporting Information. No iodine-containing compounds could be identified, and this was possibly due to their secondary photolysis yielding iodine atoms which recombine to form molecular iodine I_2. The presence of CO is likely due to the secondary photolysis of HCHO,[8] and this was also verified by subjecting gaseous HCHO to sunlight irradiation, under the same experimental conditions. Heterogeneous processes on the cell walls are not expected to significantly alter the radical oxidation mechanism proposed. Therefore, both mass spectroscopic and FT-IR analyses suggest that the reaction of CH_2I with O_2 proceeds mostly via pathways 7a and 7d.

Theoretical Calculations. All calculations were performed by density functional theory (DFT) with the Gaussian 98 program suite.[38] The B3P86 functional[39,40] was employed in all geometry optimizations, vibrational frequency, and bond strength calculations, since it was previously shown to be superior than other commonly used density functionals for the prediction of molecular geometries and the calculation of bond strengths for halogenated molecules.[41] Furthermore, it was employed in the calculation of reaction enthalpies. For all closed-shell parent molecules, the calculations were performed using restricted wavefunctions, while unrestricted wavefunctions were used for the open-shell doublet and triplet radicals.

The molecular geometry and vibrational frequency calculations were performed with the B3P86 functional in conjunction with the 6-31+G(d′,p′) basis set[42,43] for the elements H, C, O, and Cl and the SV4PD basis set[44] for iodine. All vibrational frequencies were scaled down by 0.9723 in order to account for deficiencies of the B3P86/6-31+G(d′,p′) level of theory.[41] All computed geometries were verified to be true potential energy minima, by the absence of imaginary vibrational frequencies. The calculated geometrical parameters and the harmonic vibrational frequencies for all species are shown in the Table S1 in Supporting Information.

Absolute electronic energies were subsequently obtained at higher levels of theory, comprising of the B3P86 functional in conjunction with larger basis sets. For the elements H, C, and O, a correlation-consistent basis set of triple-ζ quality augmented with diffuse functions (denoted aug-cc-pVTZ)[45,46] was considered, whereas for chlorine, the corresponding basis set possessing extra tight d-functions for second-row elements[46] were used, since this was found to be superior than the one originally constructed.[47] For iodine, the corresponding triple-ζ member of systematically convergent basis sets containing a small core pseudopotential (aug-cc-pVTZ-PP)[48] was employed.

The zero-point and the thermal energies at 298.15 K were derived by considering the harmonic oscillator and the rigid rotor approximations, and they were subsequently added to the absolute electronic energies, in order to yield the absolute enthalpies for each species, and finally, bond strengths and reaction enthalpies. In order to correct for the deficiencies of the B3P86 electronic structure calculations for open-shell species, the absolute electronic energies of all radicals were increased by the amount of $N_e(9 \times 10^{-5})$ Hartree, where N_e is the total number of electrons, as it has been suggested in a previous study.[41] Additional corrections were applied to the electronic energies for Cl and I atoms to account for the first-order spin−orbit effects in their doublet (^{2}P) ground states.[49] Therefore, the electronic energies of the Cl and I atoms were lowered by 3.5 and 30.3 kJ mol^{-1}, respectively.

The bond strengths for CH_2I_2 and the reaction enthalpies at 298.15 K for all reactions considered in the present study, calculated at the B3P86/aug-cc-pVTZ-PP level of theory, are listed in Table 3. Experimental values, derived from standard enthalpies of formation[8] are also listed for comparison. However, it has been suggested[50] that the reported experimental enthalpies of formation for CH_2I_2[51] and CHI_2[52] may be in error, therefore their calculated values at the reliable CCSD(T)/IB(DT) level of theory[50] were employed. The mean absolute deviation for 10 reaction enthalpies at the B3P86/aug-cc-pVTZ-PP level of theory from experimental or accurate ab initio values is 15.9 kJ mol^{-1}, with an average deviation of only 0.3 kJ mol^{-1}. Therefore, the uncertainty of the theoretical values in Table 3 is estimated to be in the order of 15 kJ mol^{-1}. The C−H and C−I bond strengths for CH_2I_2 at the B3P86/aug-cc-pVTZ-PP level of theory were found to be 417.0 and 207.7 kJ mol^{-1}, respectively, close to the values 426.2 and 217.7 calculated in an earlier study at the B3P86/6-311++G(2df,p) level based on MP2/6-311G(d) geometries and vibational frequencies.[41] Moreover, within estimated uncertainties, they are close to values computed at higher ab initio levels of theory: (a) 403.2 and 225.3 kJ mol^{-1}, respectively, at the CCSD(T)/IB[(DT)] level,[50] and (b) 400.3 and 215.9 kJ mol^{-1}, respectively, at the QCISD-(T)/6-311+G(3df,2p) level based on higher quality QCISD/6-311G(d,p) geometries and vibrational frequencies.[53]

TABLE 3: HI_2C-H and H_2IC-I Bond Strengths and Reaction Enthalpies at 298.15 K of CH_2I_2 with Cl Atoms, and of CH_2I and CHI_2 Radicals with O_2, at the B3P86/AUG-cc-pVTZ-PP Level of Theory[a]

reaction	experimental value[b]	calculated value
CH_2I_2 -> CHI_2 + H	403.2 ± 14.1	417.0
CH_2I_2 -> CH_2I + I	225.0 ± 12.0	207.7
CH_2I_2 + Cl -> HCl + CHI_2	−28.4 ± 14.1	−23.2
CH_2I_2 + Cl -> ICl + CH_2I	14.5 ± 12.7	3.4
CH_2I_2 + Cl -> I + CH_2ClI	−106.9 ± 14.1	−126.1
CH_2I_2 + Cl -> ICH_2I-Cl		−51.9
CHI_2 + O_2 -> I_2CHOO		−86.8
CHI_2 + O_2 -> I + ICOOH		−494.0
CHI_2 + O_2 -> IO + ICHO		−231.5
CHI_2 + O_2 -> HI + ICOO		−507.8
CHI_2 + O_2 -> HI + I + CO_2	-544.9 ± 10.0	−554.2
CHI_2 + O_2 -> OH + I_2CO		−259.5
CHI_2 + O_2 -> HO_2 + CI_2 ($^1A_1$)		170.1
CHI_2 + O_2 -> HO_2 + CI_2 ($^3B_1$)		201.2
CHI_2 + O_2 -> IOO + CHI (^{3}A″)		268.6
CHI_2 + O_2 -> IO_2 + CHI (^{3}A″)		297.5
CH_2I + O_2 -> ICH_2OO		−107.7
CH_2I + O_2 -> I + HCOOH	−489.4 ± 6.7	−467.1
CH_2I + O_2 -> IO + HCHO	−158.4 ± 6.7	−179.8
CH_2I + O_2 -> HI + HCOO	−341.8 ± 11.2	−323.9
CH_2I + O_2 -> HI + H + CO_2	−366.7 ± 6.7	−344.9
CH_2I + O_2 -> OH + ICHO		−236.6
CH_2I + O_2 -> HO_2 + CHI (^{1}A′)		234.4
CH_2I + O_2 -> HO_2 + CHI (^{3}A″)		234.3
CH_2I + O_2 -> IOO + CH_2 ($^3B_1$)		302.9
CH_2I + O_2 -> IO_2 + CH_2 ($^3B_1$)		331.9

[a] Experimentally available or accurate theoretical values are also listed for comparison. [b] Experimental values were derived from the corresponding enthalpies of formation taken from ref 8, except for CH_2I_2, CH_2ClI, and CHI_2, calculated at the CCSD(T)/IB(DT) level of theory in ref 50.

4. Discussion

The total absolute rate coefficient for the reaction of Cl atoms with CH_2I_2 was measured at four different temperatures in the range 273 − 363 K at low pressures (<3 mTorr), and the room-temperature value was $k_1 = (2.12 \pm 0.20) \times 10^{-11}$ cm^3 molecule^{-1} s^{-1}. The temperature dependence of the total rate coefficient yielded the following Arrhenius parameters: $A = (4.70 \pm 0.65) \times 10^{-11}$ cm^3 molecule^{-1} s^{-1} and $E_a = 2.00 \pm 0.27$ kJ mol^{-1}. To our knowledge, there have been only preliminary kinetic studies of the title reaction.[14,15] However, there exist kinetic studies for the reactions of Cl atoms with methane and several halogenated methanes, and relevant kinetic data along with the reaction enthalpies for abstraction of hydrogen or halogen atom by Cl atoms are listed in Table 4. The corresponding reaction enthalpies were derived using either literature values of standard enthalpies of formation,[8] or calculated values at the CCSD(T)/IB(DT) level of theory.[50]

Halomethane reactions with Cl atoms proceeding via hydrogen atom abstraction possess activation energies which tend to decrease with the number and size of halogen atom substituents, and they are all exothermic with the exception of CH_4 and CH_2F_2. On the other hand, all halogen atom abstraction pathways are increasingly endothermic as the size of the transferred halogen atom decreases. For monohalomethanes, there is no clear dependence of the Arrhenius preexponential factor on the size of the halogen atom, although a slight decrease may be noticed from CH_3F to CH_3I. However, for dihalomethanes, there is a slight increase from CH_2F_2 to CH_2Br_2, followed by a sharp increase for CH_2I_2 and CH_2ClI. The comparison of kinetic parameters between CH_3X and CH_2X_2 for the lighter alkyl halides (X = F, Cl, and Br) reveals that the second halogen

TABLE 4: Room-Temperature Rate Coefficients (k), Preexponential Arrhenius Factors (A), Activation Energies (E_a), Temperature (T), Total Pressure (P) Ranges, and Reaction Enthalpies ($\Delta^\circ H_r$) for Hydrogen/Halogen Metathesis Reactions of Chlorine Atoms with Methane and Halogenated Methanes

species	$k_{298} \times 10^{13}$ (cm^3 molecule^{-1} s^{-1})	$A \times 10^{11}$ (cm^3 molecule^{-1} s^{-1})[a]	E_a (kJ mol^{-1})[a]	T (K)[a]	P (Torr)	$\Delta^\circ H_r$ (HCl/XCl) (kJ mol^{-1})[d]	ref
CH_4	1.00	0.73	10.6			+7.5	8
	1.18	0.74	10.2	218−401	20−200		66
	1.06	0.79	10.6	218−322	5		67
	1.15	0.65/1.84	10.2/12.8	200−299/299−500	25−300		68
	1.01	0.74/1.65	10.7/12.7	220−298/298−423	1.5−4		69
	0.98	0.82/2.21	11.0/13.6	200−300/300−504	1.8−4.2		70
	0.95	0.63	10.2	221−375	50		71
	0.96	0.52/1.05	10.0/13.0	233−298/298−338	$\sim 1 \times 10^{-3}$		72
	0.99	0.70	10.6	181−291	46−68		73
	1.08	$[1.30 \times 10^{-19}\ T^{2.69}\ e^{-497/T}]$		295−1104	1.4−8.8		74
CH_3F	3.50	1.96	10.0			−7.6/+207.6	8
	3.61	0.48	6.42	216−296	5		67
	4.21	3.78	11.1	273−368	20		75
CH_3Cl	4.90	2.17	9.4			−14.4/+107.2	8
	5.10	3.36	10.4	233−322	5		67
	4.70	2.80	10.0	222−298	760		76
	5.24	$[4.00 \times 10^{-14}\ T^{0.92}\ e^{-795/T}]$		300−843	2.5−8.8		74
CH_3Br	4.40	1.40	8.6			−6.9/+77.8	8
	5.53	3.16	10.0	273−368	21		77
	4.16	1.55	8.9	222−393.5	50		78
	4.83	1.66	8.9	273−363	$\sim 1 \times 10^{-3}$		79
	4.57	$[1.02 \times 10^{-15}\ T^{1.42}\ e^{-605/T}]$		213−697	20−250		55
		pressure-dependent reversible CH_3Br-Cl adduct formation [averaged $k_{1d,T<177K} = 0.51 \times 10^{-13} \times P_{tot}$ (Torr)][b]		161−177	20−100		55
CH_3I	10.0	2.90	8.3			−9.8/+29.1	8
		5.44	10.4	364−694	25−100		21
		pressure-dependent reversible CH_3I-Cl adduct formation [$k_{1a,298} = 7.8 \times 10^{-13}$] [averaged $k_{1b,298} = 0.78 \times 10^{-13} \times P_{tot}$ (Torr)][c]		263−309	25−500		21
		irreversible pressure dependent CH_3I-Cl adduct formation [high pressure asymptote $k_{1b,T<250} \sim 300 \times 10^{-13}$][c]		218−250	5−500		21
	13.70	1.33	5.7	273−363	2×10^{-3}		19
	9.0			295	1		80
	13.5			295	700		80
	15.1			298	1.5−12		23
CF_3I	4.18	6.26	12.4	271−363	360, 700	+16.7	54
	5.10			300	2		81
	8.50			298	1.5−12		23
CH_2F_2	0.32	0.49	12.5			+0.1/+243.7	8
	0.68	2.49	14.6	273−368	20		75
CH_2Cl_2	3.50	0.74	7.6			−29.5/+91.1	8
	3.25	1.50	8.7	222−298	760		76
	3.60	$[1.48 \times 10^{-16}\ T^{1.58}\ e^{-360/T}]$		296−790	1.9−7.3		74
CH_2Br_2	4.30	0.63	6.7			−14.5/+73.6	8
	5.30	9.53	12.9	273−368	21		77
	4.14	0.63	6.7	222−394.5	50		78
	4.20	0.84	7.6	273−363	$\sim 1 \times 10^{-3}$		79
CH_2I_2	212.0	4.70	2.00	273−263	$0.5-3 \times 10^{-3}$	−28.4/+14.7	this work
	219.0	3.30	1.70	273−363	$< 3 \times 10^{-3}$		14
		[high pressure $k_{200} \sim 700 \times 10^{-13}$]		200	~20		15
CH_2ClI	850.0	4.40	−1.6	206−432	5−700	−14.2/+5.0	82
	311.0	3.13	0	273−363	$0.6-1.5 \times 10^{-3}$		22

[a] Arrhenius parameters separated by a slash correspond to each temperature range; modified Arrhenius expressions of the form $k = AT^n e^{-Ea/T}$ are explicitly shown as originally reported. [b] k_{1d} is the pressure-dependent rate coefficient for the CH_3Br-Cl adduct formation reaction, derived from the kinetic data analysis in ref 55. [c] $k_{1a,298}$ is the rate coefficient for the hydrogen metathesis reaction of reaction of CH_3I with Cl, extrapolated from the Arrhenius expression in the range 364−694 to 298 K; k_{1b} is the pressure-dependent rate coefficient for the CH_3I-Cl adduct formation reaction, derived from the kinetic data analysis in ref 21. [d] Reaction enthalpies were derived from the corresponding experimental enthalpies of formation taken from ref 8, except for CH_2I_2, CHI_2, CH_2ClI, and CHClI, calculated at the CCSD(T)/IB(DT) level of theory in ref 50.

atom leads to a decrease of reactivity, in a manner inversely dependent on the size of X. However, for iodomethanes (X = I), the presence of another halogen atom (either I or Cl) leads to an abrupt increase of reactivity as a collective effect of higher preexponential factors and lower activation energies. In addition, the reactions of CH_2I_2 and CH_2ClI with Cl atoms exhibit a significant yield for the iodine abstraction pathway, as in the case of CF_3I where only the abstraction of iodine atom is possible.[54] Moreover, in thermal reactions at ordinary temperatures, the ICl product has been observed only when the endothermicity of its formation is sufficiently low, and this may explain the absence of this pathway in the case of CH_3I, as

well as the prevalence of this pathway in the corresponding reaction of CH_2ClI.

In summary, the reactivity of Cl atoms toward iodomethanes is substantially higher than other halomethanes, in particular for the heavier molecules. The temperature dependence reveals low activation energies and high preexponential factors, suggesting the presence of attractive interactions between the two reactants and the formation of intermediate RI−Cl adducts (R = alkyl group). This behavior has been also observed in reactions of bromoalkanes with either Cl or F atoms[55,56] and in reactions of iodinated compounds with F atoms.[57,58] A comparison among the experimental or theoretically derived stabilities of the corresponding RX−Y (X = Br, I; Y = F, Cl) adducts,[20,21,55,56,58] reveals that the strength of these interactions is favored by low ionization potentials of the parent RX halides (*X* = Br, I) and large electronegativity differences between X and the incoming Y (F, Cl) halogen atoms. Thus, an apparently bimolecular reaction may have pressure-dependent contributions from more complex reaction schemes which affect the overall kinetics as well as the reaction mechanism.[21,22,55,59] At sufficiently high temperatures (related to the RX-Y bond strengths) the adducts possess very short lifetimes and these contributions are negligible. As the temperature is lowered, the adducts are able to survive longer aided by stabilizing collisions, leading to a pressure-dependent rate of their reversible formation. However, at sufficiently low temperatures and high pressures their elevated rate of irreversible formation dominates over all other atom metathesis pathways.[21,55] Structural and spectroscopic data of XCH_2I-Cl adducts (*X* = H, Cl, Br, I, CH_3, CH_3CH_2, *n*-C_3H_7, *i*-C_3H_7, *n*-C_4H_9, C_6H_5, CH_3O) have been reported in several experimental and theoretical studies.[16,17,20−22,24] In particular, the formation of the ICH_2I-Cl adduct has been recently observed at 25 − 125 Torr of N_2 over the temperature range 250−320 K by cavity ring-down spectroscopy.[16] The fluorescence spectrum of the ICH_2I-Cl adduct has been also reported, and its fluorescence lifetime at zero pressure was found to be ∼30 ns.[15] The calculated geometry of the ICH_2I-Cl adduct in the present study shows a slight perturbation of the parent CH_2I_2 structural parameters with an I−Cl bond length of 2.812 Å, a C−I−Cl bond angle of 79.89 degrees and an I−C−I−Cl dihedral angle of 180 degrees (Cl atom directed away from the other I atom). The strength of the I−Cl bond has been calculated to be 51.9 ± 15 kJ mol^{-1} at the B3P86/aug-cc-pVTZ-PP level of theory (listed in Table 3), within the range 40−60 kJ mol^{-1} computed at various ab initio and DFT (B3LYP) levels of theory for the I−Cl bond strengths of several organic iodides.[16,17,20,21,24]

The experimental results indicate that the title reaction occurs via two parallel reaction pathways: (a) the abstraction of hydrogen atom yielding HCl and CHI_2 products and (b) the abstraction of iodine atom yielding ICl and CH_2I products. The relatively high value of the rate coefficient implies that the reaction proceeds through an intermediate ICH_2I-Cl adduct, leading to an enhancement of the entropically favored iodine abstraction yield. Indeed, the relative yield measurements have shown that the ICl formation pathway contributes ca. 45 ± 10% to the total reaction rate, despite being ca. 43 kJ mol^{-1} more endothermic than H atom abstraction. In crossed molecular beam experiments,[60,61] ICl was detected following the collision of alkyl iodides with Cl atoms at high relative translational energies (over 20 kJ mol^{-1}), and the angular distribution of ICl revealed the formation of long-lived adducts which possess sufficient internal energy to dissociate via the endothermic iodine metathesis pathway. In the present case, the incoming Cl atoms may approach CH_2I_2 molecules either from the methylene side and result in the direct abstraction of a hydrogen atom yielding HCl and CHI_2, or from the iodine side and form the ICH_2I-Cl adduct which subsequently undergoes scission of the C−I bond yielding ICl or four-center elimination of HCl. In particular for the low-pressure regime explored in the present study, weakly bound adducts are not expected to be efficiently stabilized by collisions, and may rapidly dissociate back to reactants or yield the reaction products.

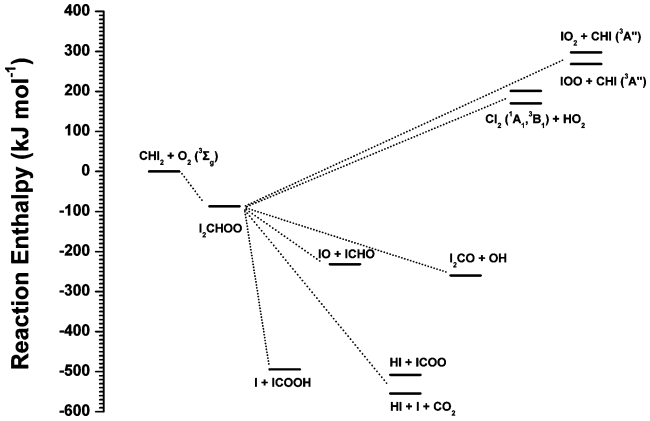

Figure 5. Reaction enthalpy diagram (in kJ mol^{-1}), calculated at the B3P86/aug-cc-pVTZ-PP level of theory, for the reaction pathways of CHI_2 radical with molecular O_2.

The formation enthalpies calculated for the ICH_2I-Cl and CH_3I-Cl adducts are comparable,[20,21] suggesting that the onset of pressure dependence in the rate coefficients of the title reaction may occur at temperatures below ca. 360 K, as observed for the reaction of CH_3I with Cl atoms.[21] As shown in Table 4, the decomposition pathways of the ICH_2I-Cl adduct to HCl or ICl are thermochemically more favorable than those of CH_3I-Cl, implying lower unimolecular reaction barriers, faster forward rates, and consequently, shorter lifetimes. Therefore, ICH_2I-Cl appears to be less stable than CH_3I-Cl in respect to decomposition pathways accessible, which would direct the onset of pressure dependence at a lower temperature than CH_3I + Cl, and possibly, out of the temperature range 273−363 K, employed in this study. Indeed, the ICH_2I-Cl adduct was recently reported to undergo significant unimolecular dissociation to products at 296 K, and the data do not suggest regeneration of reactants.[15] However, at 200 K the reaction mechanism is similar to that of CH_3I, and the LIF temporal profile of ICH_2I-Cl suggests a high-pressure rate coefficient for adduct formation of $\sim 7 \times 10^{-11}$ cm^3 $molecule^{-1}$ s^{-1}, a factor of 2 higher than CH_3I + Cl. In our system, it is not possible to examine the bimolecular reaction rate coefficients dependence on total pressure due to the very nature of the VLPR technique which limits the operating range to several mTorr. Mass spectrometric detection of weakly bound adducts by their parent ions is also unlikely because of their fragmentation which is expected to occur even at the lowest electron energies attainable.

The oxidation mechanism of the CHI_2 and CH_2I radicals by molecular O_2 was also considered in the present study, in an attempt to resolve inconsistencies between the proposed mechanism in two previous studies.[27,28] The reaction enthalpy diagrams for the radical oxidation pathways, calculated at the B3P86/aug-cc-pVTZ-PP level of theory, are shown in Figures 5 and 6, for CHI_2 and CH_2I, respectively. The initial step is assumed to be the formation of the corresponding peroxy radicals, which subsequently undergo unimolecular dissociation to oxidation products.

The qualitative product analysis by either mass spectrometry at low pressures or IR spectroscopy at nearly atmospheric

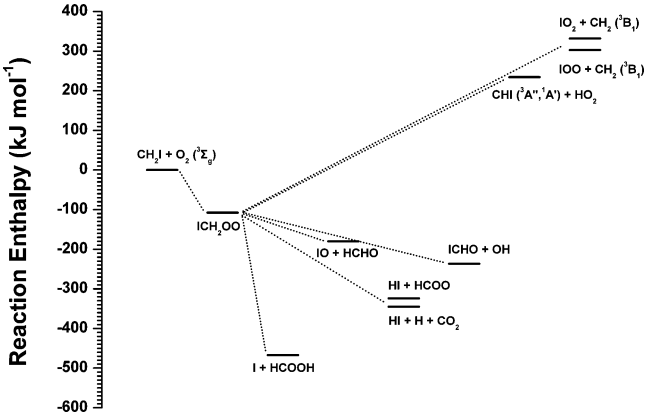

Figure 6. Reaction enthalpy diagram (in kJ mol^{-1}), calculated at the B3P86/aug-cc-pVTZ-PP level of theory, for the reaction pathways of CH_2I radical with molecular O_2.

pressures suggests that HCOOH and HCHO are among the final products of iodomethyl radicals oxidation by O_2. In an early work, CH_2I_2 was photolyzed at 300 nm, and I_2, HCHO, HCOOH, and $(CH_2O)_2$ were identified as oxidation products by visible and near-UV absorption.[62] In chamber experiments, the photolysis ($\lambda = 320-480$ nm) of a mixture of CH_2I_2 and O_3 in synthetic air was found to yield CO, HCHO, HCOOH, and $(HCO)_2O$, detected by long-path FT-IR.[63] In a recent work employing cavity ring-down spectroscopy, the relative yield of iodine monoxide IO was determined by the oxidation of CH_2I radicals generated by CH_2I_2 photolysis at 266 nm; it was reported that the $CH_2I + O_2$ reaction proceeds exclusively via pathway 7a leading to IO + HCHO, by titrating the IO radicals using as reference the reactions of CH_3I/CF_3I with $O(^3P)$ atoms.[27] In another work, CH_2I radicals were generated by photolyzing CH_2I_2 at 248 nm and the oxidation products were found to be iodine atoms and IO radicals by photoionization mass spectrometry; however, no HCHO or HCOOH were detected, which was attributed to a low sensitivity for these molecules.[28] In a recent work, the yield of IO from the reactions of longer iodoalkyl radicals $C_nH_{2n+1}CHI$ ($n = 1-3$, generated by H atom abstraction from the corresponding iodoalkanes using Cl atoms) was found to be 0.05−0.15, by cavity ring-down spectroscopy.[29] These low IO yields were attributed to stabilization of the iodoalkylperoxy radicals $C_nH_{2n+1}CHIOO$ and to a less preferential generation of the α-radicals $C_nH_{2n+1}CHI$ by H atom abstraction from long alkyl chains. The exclusive production of IO by the reaction of CH_2I radical with O_2 reported previously[27] contradicts all other studies, including the present one, which indicate that at least two pathways of the CH_2I oxidation (7a and 7d) are accessible, yielding IO + HCHO and I + HCOOH, respectively. Moreover, the results of Eskola et al.[28] suggest that iodine atom generation (pathway 7d) dominates over IO generation (pathway 7a). The relative reaction enthalpies for these two pathways, as shown in Table 3, suggest a less thermochemically favorable IO formation, since pathway 7d was found to be significantly (ca. 300 kJ mol^{-1}) more exothermic than pathway 7a. However, discrepancies between the proposed mechanisms may arise from variations of the energy content of the nascent CH_2I radical, affecting its reactivity and the relative yields for the unimolecular decomposition pathways of iodomethyl peroxy radical ICH_2OO.

Considering the tropospheric chemistry of CH_2I_2, photolysis by sunlight constitutes the main removal process of CH_2I_2 in the marine boundary layer, with an estimated lifetime at midday of about 5 min.[64,65] The rate coefficient of the title reaction at room temperature and at low pressures of 2.12×10^{-11} cm^3 molecule^{-1} s^{-1} corresponds to a much longer corresponding lifetime of 6 days, by using the maximum concentration levels of Cl atoms at coastal sites of ca. 1×10^5 molecule cm^{-3}.[5,7] However, at atmospheric pressures and lower temperatures, a contribution from the adduct formation pathway may increase the total rate coefficient of the CH_2I_2 loss by Cl atoms to an estimated value of $\sim 7 \times 10^{-11}$ cm^3 molecule^{-1} s^{-1},[15] with a corresponding lifetime of about 40 h, still substantially longer than its photolysis lifetime. Thus, the reaction with chlorine atoms may be considered to be a negligible sink of CH_2I_2 in the atmosphere. Furthermore, no substantial amounts of CHI_2 radicals are expected to be produced by the degradation of CH_2I_2, and the subsequent oxidation chemistry will be carried over by the photolytically generated CH_2I radicals.

5. Conclusions

The gas-phase reaction of CH_2I_2 with Cl atoms at the mTorr pressure regime proceeds via hydrogen (55%) and iodine (45%) atom metathesis with a total rate coefficient of $(2.12 \pm 0.06) \times 10^{-11}$ cm^3 molecule^{-1} s^{-1} at 303 K. It is one of the fastest reactions of Cl atoms with alkyl halides, assisted by attractive interactions between the reactants leading to the ICH_2I-Cl adduct, with a calculated I−Cl bond strength of 51.9 kJ mol^{-1}. However, the contribution of the reaction to the total tropospheric loss of CH_2I_2 is negligible owing to the rapid photolysis of CH_2I_2. Thus, CH_2I radicals are the primary products of CH_2I_2 degradation in the marine boundary layer, which in turn react with atmospheric oxygen to yield mainly iodine atoms, IO radicals, HCOOH and HCHO.

Acknowledgment. This work was supported by the Greek Secretariat of Research and Technology within the project TROPOS (2005-2006), and by the Cyprus Research Promotion Foundation within the project APOIKOS (2006-2007). Theoretical work was partially supported by the "Excellence in the Research Institutes" Program, Action 3.3.1, which was cofunded by the Greek Secretariat of Research and Technology (GSRT) and the European Union (EU).

Supporting Information Available: A typical calibration plot for Cl atoms, an FT-IR spectrum of a photolyzed CH_2I_2 and O_2 mixture, and a table listing the calculated geometrical parameters and harmonic vibrational frequencies. This information is available free of charge via the Internet at http://pubs.acs.org.

References and Notes

(1) Brasseur, G. P.; Orlando, J. J.; Tyndall, G. S. *Atmospheric Chemistry and Global Change*; Oxford University Press: New York, 1999.

(2) Carpenter, L. *J. Chem. Rev.* **2003**, *103*, 4953.

(3) Davis, D.; Crawford, J.; Liu, S.; McKeen, S.; Bandy, A.; Thornton, D.; Rowland, F. S.; Blake, D. *J. Geophys. Res.* **1996**, *101*, 2135.

(4) Vogt, R.; Sander, R.; Von Glasow, R.; Crutzen, P. J. *J. Atmos. Chem.* **1999**, *32*, 375.

(5) Spicer, C. W.; Chapman, E. G.; Finlayson-Pitts, B. J.; Plastridge, R. A.; Hubbe, J. M.; Fast, J. D.; Berkowitz, C. M. *Nature* **1998**, *394*, 353.

(6) Finlayson-Pitts, B. J.; Ezell, M. J.; Pitts, J. N. J. *Nature* **1989**, *337*, 241.

(7) Keene, W. C.; Stutz, J.; Pszenny, A. A. P.; Maben, J. R.; Fischer, E. V.; Smith, A. M.; von Glasow, R.; Pechtl, S.; Sive, B. C.; Varner, R. K. *J. Geophys. Res.* **2007**, *112*, D10S12.

(8) Sander, S. P.; Friedl, R. R.; Ravishankara, A. R.; Golden, D. M.; Kolb, C. E.; Kurylo, M. J.; Molina, M. J.; Moortgat, G. K.; Keller-Rudek, H.; Finlayson-Pitts, B. J.; Wine, P. H.; Huie, R. E.; Orkin, V. L. *Chemical Kinetics and Photochemical Data for Use in Atmospheric Studies, Evaluation Number 15, Publication 06−2*; Jet Propulsion Laboratory (JPL); California Institute of Technology: Pasadena, CA, 2006.

(9) Kolb, C. E. *Nature* **2002**, *417*, 597.

(10) O'Dowd, C. D.; Jimenez, J. L.; Bahreini, R.; Flagan, R. C.; Seifeld, J. H.; Haameri, K.; Pirjola, L.; Kulmala, M.; Jennings, S. G.; Hoffmann, T. *Nature* **2002**, *417*, 632.

(11) McFiggans, G.; Coe, H.; Burgess, R.; Allan, J.; Cubison, M.; Alfarra, M. R.; Saunders, R.; Saiz-Lopez, A.; Plane, J. M. C.; Wevill, D. J.; Carpenter, L. J.; Rickard, A. R.; Monks, P. S. *Atmos. Chem. Phys.* **2004**, *4*, 701.

(12) Saiz-Lopez, A.; Plane, J. M. C.; McFiggans, G.; Williams, P. I.; Ball, S. M.; Bitter, M.; Jones, R. L.; Hongwei, C.; Hoffmann, T. *Atmos. Chem. Phys.* **2006**, *6*, 883.

(13) Jimenez, J. L.; Cocker, D. R.; Bahreini, R.; Zhuang, H.; Varutbangkul, V.; Flagan, R. C.; Seinfeld, J. H.; Hoffmann, T.; O'Dowd, C. D. *J. Geophys. Res.* **2003**, *108*, 4318.

(14) Stefanopoulos, V. G.; Papadimitriou, V. C.; Lazarou, Y. G.; Papagiannakopoulos, P. *Geophys. Res. Abstr.* **2003**, *5*, 12095.

(15) Gravestock, T.; Blitz, M.; Sharma, R.; Pilling, M.; Seakins, P.; Heard, D. *19th International Symposium on Gas Kinetics*; Universite d'Orléans, Polytech'Orléans: Orléans, 2006.

(16) Enami, S.; Hashimoto, S.; Kawasaki, M.; Nakano, Y.; Ishiwata, T.; Tonokura, K.; Wallington, T. J. *J. Phys. Chem. A* **2005**, *109*, 1587.

(17) Enami, S.; Yamanaka, T.; Hashimoto, S.; Kawasaki, M. *J. Phys. Chem. A* **2005**, *109*, 6066.

(18) Kambanis, K. G.; Lazarou, Y. G.; Papagiannakopoulos, P. *Chem. Phys. Lett.* **1996**, *261*, 457.

(19) Kambanis, K. G.; Lazarou, Y. G.; Papagiannakopoulos, P. *Chem. Phys. Lett.* **1997**, *268*, 498.

(20) Lazarou, Y. G.; Kambanis, K. G.; Papagiannakopoulos, P. *Chem. Phys. Lett.* **1997**, *271*, 280.

(21) Ayhens, Y. V.; Nicovich, J. M.; McKee, M. L.; Wine, P. H. *J. Phys. Chem. A* **1997**, *101*, 9382.

(22) Kambanis, K. G.; Argyris, D. Y.; Lazarou, Y. G.; Papagiannakopoulos, P. *J. Phys. Chem. A* **1999**, *103*, 3210.

(23) Cotter, E. S. N.; Booth, N. J.; Canosa-Mas, C. E.; Gray, D. J.; Shallcross, D. E.; Wayne, R. P. *Phys. Chem. Chem. Phys.* **2001**, *3*, 402.

(24) Orlando, J. J.; Piety, C. A.; Nicovich, J. M.; McKee, M. L.; Wine, P. H. *J. Phys. Chem A* **2005**, *109*, 6659.

(25) Cotter, E. S. N.; Booth, N. J.; Canosa-Mas, C. E.; Wayne, R. P. *Atmos. Environ.* **2001**, *35*, 2169.

(26) Sehested, J.; Ellermann, T.; Nielsen, O. J. *Int. J. Chem. Kinet.* **1994**, *26*, 259.

(27) Enami, S.; Ueda, J.; Goto, M.; Nakano, Y.; Aloisio, S.; Hashimoto, S.; Kawasaki, M. *J. Phys. Chem. A* **2004**, *108*, 6347.

(28) Eskola, A. J.; Wojzik-Pastuszka, D.; Ratajczak, E.; Timonen, R. S. *Phys. Chem. Chem. Phys.* **2006**, *8*, 1416.

(29) Enami, S.; Yamanaka, T.; Hashimoto, S.; Kawasaki, M.; Tonokura, K.; Tachikawa, H. *Chem. Phys. Lett.* **2007**, *445*, 152.

(30) Masaki, A.; Tsunashima, S.; Washida, N. *J. Phys. Chem.* **1995**, *99*, 13126.

(31) Papadimitriou, V. C.; Prosmitis, A. V.; Lazarou, Y. G.; Papagiannakopoulos, P. *J. Phys. Chem. A* **2003**, *107*, 3733.

(32) Chesnokov, E. N. *Khim. Fiz.* **1991**, *10*, 204.

(33) Papadimitriou, V. C.; Papanastasiou, D. K.; Stefanopoulos, V. G.; Zaras, A. M.; Lazarou, Y. G.; Papagiannakopoulos, P. *J. Phys. Chem. A* **2007**, *111*, 11608.

(34) Yuan, J.; Misra, A.; Goumri, A.; Shao, D. D.; Marshall, P. *J. Phys. Chem. A* **2004**, *108*, 6857.

(35) Bedjanian, Y.; Le, Bras, G.; Poulet, G. *J. Phys. Chem. A* **1996**, *100*, 15130.

(36) Vipond, A.; Canosa-Mas, C. E.; Flugge, M. L.; Gray, D. J.; Shallcross, D. E.; Shah, D.; Wayne, R. P. *Phys. Chem. Chem. Phys.* **2002**, *4*, 3648.

(37) NIST Standard Reference Database Number 69 - February 2000 Release; NIST: Gathersberg, MD.

(38) Frisch, M. J.; Trucks, G. W.; Schlegel, H. B.; Scuseria, G. E.; Robb, M. A.; Cheeseman, J. R.; Zakrzewski, V. G.; Montgomery, J. A., Jr.; Stratmann, R. E.; Burant, J. C.; Dapprich, S.; Millam, J. M.; Daniels, A. D.; Kudin, K. N.; Strain, M. C.; Farkas, O.; Tomasi, J.; Barone, V.; Cossi, M.; Cammi, R.; Mennucci, B.; Pomelli, C.; Adamo, C.; Clifford, S.; Ochterski, J.; Petersson, G. A.; Ayala, P. Y.; Cui, Q.; Morokuma, K.; Malick, D. K.; Rabuck, A. D.; Raghavachari, K.; Foresman, J. B.; Cioslowski, J.; Ortiz, J. V.; Stefanov, B. B.; Liu, G.; Liashenko, A.; Piskorz, P.; Komaromi, I.; Gomperts, R.; Martin, R. L.; Fox, D. J.; Keith, T.; Al-Laham, M. A.; Peng, C. Y.; Nanayakkara, A.; Gonzalez, C.; Challacombe, M.; Gill, P. M. W.; Johnson, B. G.; Chen, W.; Wong, M. W.; Andres, J. L.; Head-Gordon, M.; Replogle, E. S.; Pople, J. A. *Gaussian 98*, revision A.9; Gaussian, Inc.: Pittsburgh, PA, 1998.

(39) Becke, A. D. *J. Chem. Phys.* **1993**, *98*, 5648.

(40) Perdew, J. P.; Burke, K.; Wang, Y. *Phys. Rev. B* **1996**, *54*, 16533.

(41) Lazarou, Y. G.; Prosmitis, A. V.; Papadimitriou, V. C.; Papagiannakopoulos, P. *J. Phys. Chem. A* **2001**, *105*, 6729.

(42) Petersson, G. A.; Al-Laham, M. A. *J. Chem. Phys.* **1991**, *94*, 6081.

(43) Petersson, G. A.; Bennett, A.; Tensfeld, T. G.; al-Laham, M. A.; Shirley, W. A.; Mantziaris, J. *J. Chem. Phys.* **1988**, *89*, 2193.

(44) Andzelm, J.; Klobukowski, M.; Radzio-Andzelm, E. *J. Comput. Chem.* **1984**, *5*, 146.

(45) Dunning, T. H., Jr. *J. Chem. Phys.* **1989**, *90*, 1007.

(46) Dunning, T. H., Jr.; Peterson, K. A.; Wilson, A. K. *J. Chem. Phys.* **2001**, *114*, 9244.

(47) Woon, D.; Dunning, T. H., Jr. *J. Chem. Phys.* **1993**, *98*, 1358.

(48) Peterson, K. A.; Figgen, D.; Goll, E.; Stoll, H.; Dolg, M. *J. Chem. Phys.* **2003**, *119*, 11113.

(49) Moore, C. E. *Atomic Energy Levels*; Vol. U.S. National Bureau of Standards Circular 37; NBS: Washington, DC, 1971.

(50) Lazarou, Y. G.; Papadimitriou, V. C.; Prosmitis, A. V.; Papagiannakopoulos, P. *J. Phys. Chem. A* **2002**, *106*, 11502.

(51) Kudchadker, S. A.; Kudchadker, A. P. *J. Phys. Chem. Ref. Data* **1976**, *5*, 529.

(52) *CRC Handbook of Chemistry and Physics*, 76th ed.; CRC Press: Boca Raton, FL, 1995.

(53) Marshall, P.; Srinivas, G. N.; Schwartz, M. *J. Phys. Chem A* **2005**, *109*, 6371.

(54) Kaiser, E. W.; Wallington, T. J.; Hurley, M. D. *Int. J. Chem. Kinet.* **1995**, *27*, 205.

(55) Piety, C. A.; Soller, R.; Nicovich, J. M.; McKee, M. L.; Wine, P. H. *Chem. Phys.* **1998**, *231*, 155.

(56) Sehested, J.; Bilde, M.; Møgelberg, T.; Wallington, T. J.; Nielsen, O. J. *J. Phys. Chem.* **1996**, *100*, 10989.

(57) Farrar, J. M.; Y. T., L. *J. Chem. Phys.* **1975**, *63*, 3639.

(58) White, R. W. P.; Smith, D. J.; Grice, R. *J. Phys. Chem.* **1993**, *97*, 2123.

(59) Mozurkewich, M.; Benson, S. W. *J. Phys. Chem* **1984**, *88*, 6429.

(60) Hoffmann, S. M. A.; Smith, D. J.; Ureña, A. G.; Steele, T. A.; Grice, R. *Mol. Phys.* **1984**, *53*, 1067.

(61) Hoffmann, S. M. A.; Smith, D. J.; González, Ureña, A.; Grice, R. *Chem. Phys. Lett.* **1984**, *107*, 99.

(62) Schmitt, G.; Comes, F. J. *J. Photochem.* **1980**, *14*, 107.

(63) Barnes, I.; Bastian, V.; Becker, K. H. *Physico-chemical behaviour of atmospheric pollutants*; Kluwer: Dordrecht, 1990.

(64) Roehl, C. M.; Burkholder, J. B.; Moortgat, G. K.; Ravishankara, A. R.; Crutzen, P. J. *J. Geophys. Res.* **1997**, *102*, 12819.

(65) Mössinger, J.; Shallcross, D. E.; Cox, R. A. *J. Chem. Soc. Faraday Trans.* **1998**, *10*, 1391.

(66) Watson, R. G. M.; Fischer, S.; Davis, D. D. *J. Chem. Phys.* **1976**, *65*, 2126.

(67) Manning, R. G.; Kurylo, M. J. *J. Phys. Chem.* **1977**, *81*, 291.

(68) Whytock, D. A.; Lee, J. H.; Michael, J. V.; Payne, W. A.; Stief, L. J. *J. Chem. Phys.* **1977**, *66*, 2690.

(69) Keyser, L. F. *J. Chem. Phys.* **1978**, *69*, 214.

(70) Zahniser, M. S.; Berquist, B. M.; Kaufman, F. *Int. J. Chem. Kinet.* **1978**, *10*, 15.

(71) Ravishankara, A. R.; Wine, P. H. *J. Chem. Phys.* **1980**, *72*, 25.

(72) Heneghan, S. P.; Knoot, P. A.; Benson, S. W. *Int. J. Chem. Kinet.* **1981**, *13*, 677.

(73) Seeley, J. V.; Jayne, J. T.; Molina, M. J. *J. Phys. Chem.* **1996**, *100*, 4019.

(74) Bryukov, M. G.; Slagle, I. R.; Knyazev, V. D. *J. Phys. Chem. A* **2002**, *106*, 10532.

(75) Tschuikow-Rouw, E.; Yano, T.; Niedzielski, J. *J. Chem. Phys.* **1985**, *82*, 65.

(76) Orlando, J. J. *Int. J. Chem. Kinet.* **1999**, *31*, 515.

(77) Tschuikow-Rouw, E.; Faraji, F.; Paddison, S.; Niedzielski, J.; Miyokawa, K. *J. Phys. Chem.* **1988**, *92*, 1488.

(78) Gierczak, T.; Goldfarb, L.; Sueper, D.; Ravishankara, A. R. *Int. J. Chem. Kinet.* **1994**, *26*, 719.

(79) Kambanis, K. G.; Lazarou, Y. G.; Papagiannakopoulos, P. *J. Phys. Chem. A* **1997**, *101*, 8496.

(80) Bilde, M.; Wallington, T. J. *J. Phys. Chem. A* **1998**, *102*, 1550.

(81) Manke, G. C. I.; Setser, D. W. *J. Phys. Chem. A* **1998**, *102*, 153.

(82) Bilde, M.; Sehested, J.; Nielsen, O. J.; Wallington, T. J.; Meagher, R. J.; McIntosh, M. E.; Piety, C. A.; Nicovich, J. M.; Wine, P. H. *J. Phys. Chem. A* **1997**, *101*, 8035.